Available online at www.sciencedirect.com
ScienceDirect
Geochimica et Cosmochimica Acta 74 (2010) 3459–3475
Geochimica et Cosmochimica Acta
www.elsevier.com/locate/gca

Lithium isotope geochemistry of marine pore waters – Insights from cold seep fluids

Florian Scholz [a,*], Christian Hensen [a], Gert J. De Lange [b], Matthias Haeckel [a], Volker Liebetrau [a], Anette Meixner [c], Anja Reitz [a], Rolf L. Romer [c]

[a] Leibniz-Institute of Marine Sciences, IFM-GEOMAR, Wischhofstraße 1-3, D-24148 Kiel, Germany
[b] Utrecht University, Faculty of Geosciences, Department of Earth Sciences – Geochemistry, P.O. Box 80021, 3508 TA Utrecht, The Netherlands
[c] Deutsches GeoForschungsZentrum GFZ, Telegrafenberg, D-14473 Potsdam, Germany

Received 24 November 2009; accepted in revised form 23 March 2010; available online 30 March 2010

Abstract

Lithium concentration and isotope data (δ^7Li) are reported for pore fluids from 18 cold seep locations together with reference fluids from shallow marine environments, a sediment-hosted hydrothermal system and two Mediterranean brine basins. The new reference data and literature data of hydrothermal fluids and pore fluids from the Ocean Drilling Program follow an empirical relationship between Li concentration and δ^7Li ($\delta^7\text{Li} = -6.0(\pm 0.3) \cdot \ln[\text{Li}] + 51(\pm 1.2)$) reflecting Li release from sediment or rocks and/or uptake of Li during mineral authigenesis. Cold seep fluids display δ^7Li values between +7.5‰ and +45.7‰, mostly in agreement with this general relationship. Ubiquitous diagenetic signals of clay dehydration in all cold seep fluids indicate that authigenic smectite–illite is the major sink for light pore water Li in deeply buried continental margin sediments. Deviations from the general relationship are attributed to the varying provenance and composition of sediments or to transport-related fractionation trends. Pore fluids on passive margins receive disproportionally high amounts of Li from intensely weathered and transported terrigenous matter. By contrast, on convergent margins and in other settings with strong volcanogenic input, Li concentrations in pore water are lower because of intense Li uptake by alteration minerals and, most notably, adsorption of Li onto smectite. The latter process is not accompanied by isotope fractionation, as revealed from a separate study on shallow sediments. A numerical transport-reaction model was applied to simulate Li isotope fractionation during upwelling of pore fluids. It is demonstrated that slow pore water advection (order of mm a^{-1}) suffices to convey much of the deep-seated diagenetic Li signal into shallow sediments. If carefully applied, Li isotope systematics may, thus, provide a valuable record of fluid/mineral interaction that has been inherited several hundreds or thousands of meters below the actual seafloor fluid escape structure.

1. INTRODUCTION

In the past two decades, the behavior of Li isotopes has been studied in various marine systems, including mid-ocean ridge and sediment-hosted hydrothermal systems (Chan et al., 1993, 1994; James et al., 1999), subduction zone settings (You et al., 1995; Chan and Kastner, 2000) and normal coastal and deep-sea sediments recovered by means of deep-sea drilling (Zhang et al., 1998; James and Palmer, 2000). Major processes identified to cause deviations from the seawater isotopic composition are adsorption/desorption reactions (Zhang et al., 1998; James and Palmer, 2000), formation and transformation of silicate minerals (Chan and Kastner, 2000; Williams and Hervig, 2005) and leaching of Li from sediments or underlying crust at high temperature (Martin et al., 1991; Chan et al., 1993, 1994; James et al., 1999). As a result of the accomplished

* Corresponding author. Tel.: +49 431 6002562; fax: +49 431 6002915.
E-mail address: fscholz@ifm-geomar.de (F. Scholz).

0016-7037/$ - see front matter © 2010 Elsevier Ltd. All rights reserved.
doi:10.1016/j.gca.2010.03.026

work, Li isotopes are considered a promising tracer for the diagenetic evolution and provenance of pore fluids in overpressured sedimentary environments.

The Li isotopic composition of seawater (δ^7Li: +31‰; Millot et al., 2004) is distinct from mid-ocean ridge basalt (MORB) (δ^7Li: $+3.4 \pm 1.4$‰; Tomascak et al., 2008) and clastic, marine sediments (δ^7Li: −1.5‰ to +5‰; Chan et al., 2006) and the direction of Li exchange among these reservoirs is temperature-dependent. Under normal seafloor conditions, seawater Li is sequestered by authigenic clay minerals. Since the light isotope, ^{6}Li, is preferentially taken up, the remaining Li-depleted fluids become isotopically heavier during this process. By contrast, at elevated temperatures, simultaneous leaching of Li from primary minerals and uptake into secondary minerals shifts the Li isotope value of fluids between that of seawater and the initial solid (e.g., Chan et al., 1993, 1994; Zhang et al., 1998; James et al., 2003). Since both the distribution coefficient between solid and fluid and the extent of isotope fractionation during mineral authigenesis are a function of temperature (Berger et al., 1988; Chan et al., 1994), mobile fluids in porous media may undergo multiple stages of Li uptake and loss. The complex Li isotope signature resulting from this bears a valuable record of fluid/mineral interaction that is, however, challenging to unravel.

To better constrain the Li isotope signature of advecting pore fluids in continental margin sediments, pore water samples from 18 cold seep locations in varying geological settings were analyzed for their Li concentration and isotopic composition. Literature data of hydrothermal fluids and pore waters from the Ocean Drilling Program (ODP) were compiled in order to establish a frame of reference for Li isotope exchange between fluids and solids in related marine systems. Comparison of the presented results with that reference frame yields insights into the provenance and diagenetic evolution of cold seep fluids. Two evolutionarily distinct Messinian brines from the Mediterranean Sea were included in this study to test whether hypersaline pore fluids are subject to specific fractionation mechanisms. Eventually, a transport-reaction model is used to retrace fractionation trends during upwelling of fluids to the seafloor. Besides being of relevance to studies on the origin and evolution of cold seep fluids, this article reviews general principles for the interpretation of Li isotope variations in the context of diagenesis and pore water/mineral interaction in marine sediments.

2. SAMPLES

The following section gives a brief overview about the geological context of the studied seepage areas (Fig. 1) and chemical characteristics of the pore fluids. More detailed information may be obtained from the references cited in the text. The geographical position and water depth of the sampling locations are summarized in Table 1.

2.1. Regional settings

Upward movement of overpressured fluids is often associated with compressional tectonics and subduction related processes (Hyndman and Davis, 1992). Mound 11, Mud Pie and Mound Ridge are cold seeps on the Central American margin (map 1 in Fig. 1) where the Cocos plate

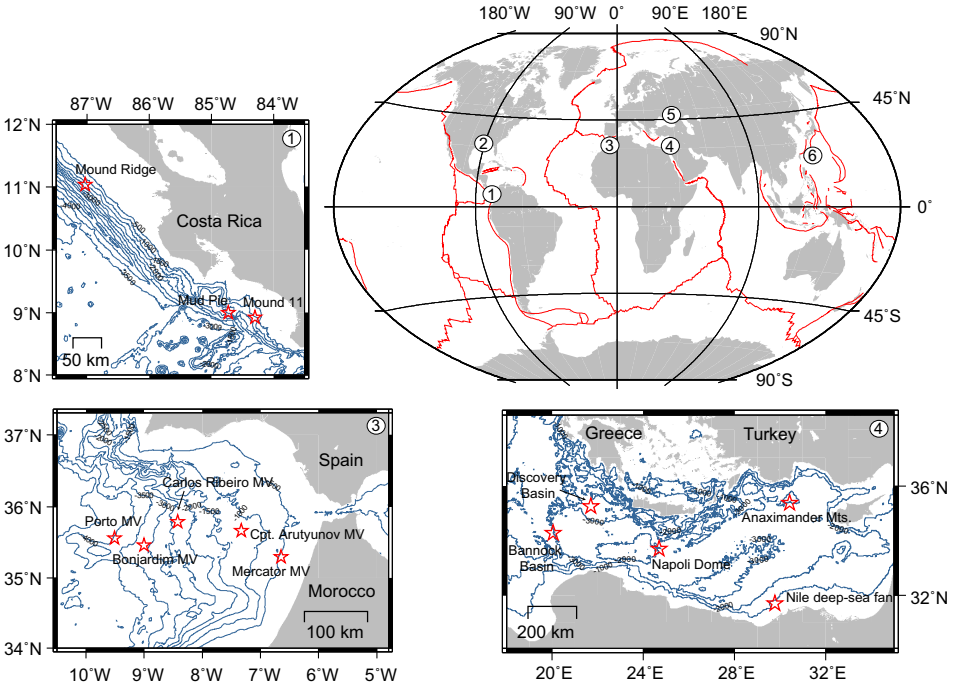

Fig. 1. Global map showing the study areas (1) Central American margin, (2) Gulf of Mexico, (3) Gulf of Cadiz, (4) Eastern Mediterranean Sea, (5) Black Sea and (6) Okinawa Trough. Major tectonic plate boundaries are represented by thin lines. Detailed maps with bathymetric information are shown for (1), (3) and (4). Stars indicate the position of sampling sites or sub-regions. See Table 1 for geographical positions and water depths.

Table 1
General characteristics of the sampling sites and sediment cores.

Area	Location	Cruise	Station/sampling device[b]	Latitude	Longitude	Water depth (m)
Reference sites						
Gulf of Cadiz	Reference core	MSM1-3	139-MUC2	35°27.56′N	8°59.88′W	3054
Nile deep-sea fan	Reference core	POS362-2	MUC28	31°41.58′N	29°46.07′E	725
(E Mediterranean Sea)	Reference core	POS362-2	GC2	31°41.63′N	29°46.10′E	722
Black Sea	Reference core	M72-3	GeoB11905 (MIC)	41°57.43′N	41°16.80E	877
	Reference core	M72-3	GeoB11974 (GC)	41°57.43′N	41°16.80′E	884
Okinawa Trough	Abyss Vent[a]	SO196	95MUC28	24°50.78′N	122°42.03′E	1394
(NW Pacific Ocean)	Abyss Vent[a]	SO196	44PC33	24°50.78′N	122°42.03′E	~1390
	Swallow chimney[a]	SO196	34GC1	24°50.84′N	122°42.00′E	1382
E Mediterranean Sea	Discovery brine	PaleoPass04	28CT (rosette)	35°16.62′N	21°41.45′E	
	Bannock brine	PaleoPass04	09CT (rosette)	34°17.99′N	20°01.72′E	
Seep sites						
Central American margin	Mound 11	SO173	TVMUC127	8°55.31′N	84°18.22′W	1012
(E equatorial Pacific)	Mud Pie	M66	108/78/27 (PC)	8°59.60′N	84°43.68′W	1917
	Mound Ridge	M66	GC219	11°02.45′N	87°02.16′W	1710
Gulf of Mexico	Green Canyon 415 East	SO174	TGC3	27°32.61′N	90°59.55′W	353
	Green Canyon Bush Hill	SO174	GC8	27°46.98′N	91°30.47′W	553
Gulf of Cadiz	Porto MV	MSM1-3	143GC3	35°33.70′N	9°30.44′W	3860
(NE Atlantic Ocean)	Bonjardim MV	MSM1-3	130GC1	35°27.82′N	9°00.14′W	3049
	Carlos Ribeiro MV	MSM1-3	154GC5	35°47.26′N	8°25.36′W	2198
	Captain Arutyunov MV	MSM1-3	174-GC9	35°39.74′N	7°19.96′W	1322
	Captain Arutyunov MV	MSM1-3	205GC13	35°39.70′N	7°20.08′W	1326
	Mercator MV	MSM1-3	239-GC20	35°17.92′N	6°38.70′W	353
	Mercator MV	MSM1-3	263-GC28	35°17.87′N	6°38.80′W	351
E Mediterranean Sea	Napoli Dome	MD69	KC11 (PiC)	33°43.28′N	24°41.27′E	1925
	Kazan MV	Aegeo04	18GC1	35°25.91′N	30°33.71′E	1696
	Kazan MV	MIMES04	07GT (GC)	35°25.92′N	30°33.71′E	1663
	Amsterdam MV	Aegeo04	02AP2 (GC)	35°20.00′N	30°16.28′E	2030
	Amsterdam MV	Aegeo04	02AP3 (GC)	35°20.00′N	30°16.24′E	2022
	Giza MV	POS362-2	GC5	31°40.51′N	29°45.00′E	666
	Giza MV	POS362-2	GC34	31°40.54′N	29°45.24′E	671
	North Alex MV	POS362-2	GC100	31°58.16′N	30°08.16′E	483
Black Sea	Dvurechenskii MV	M72-3	GeoB11977 (MIC)	44°16.89′N	34°58.91′E	2052
	Dvurechenskii MV	M72-3	GeoB11978 (MIC)	44°16.94′N	34°58.90′E	2050
	Pechori Mound	M72-3	GeoB11955 (GC)	41°58.96′N	41°07.54′E	1012

[a] Sediment cores were retrieved in the vicinity of the identically named hydrothermal vent structures.
[b] MUC, multi corer; PC, push core; GC, gravity corer; PiC, piston corer; MIC, mini corer.

is subducted beneath the Caribbean plate (Ranero and Von Huene, 2000; Hensen et al., 2004). Fluid seepage and mud volcanism on the Mediterranean Ridge is related to subduction of the African plate beneath the Eurasian plate (Camerlenghi et al., 1992; Robertson et al., 1996; Robertson and Kopf, 1998). The major mud volcano (MV) areas on the Mediterranean Ridge are the Olimpi Field on the accretionary prism south of Crete (Napoli Dome) and, further east, the Anaximander Mountains (Kazan and Amsterdam MVs) located at the junction of the Hellenic and Cyprus Arcs (map 4 in Fig. 1; Zitter et al., 2005). Although not directly related to subduction, mud volcanism in the Black Sea (Dvurechenskii MV and Pechori Mound) also occurs in the tectonic context of plate convergence between Africa and Eurasia (Limonov et al., 1997; Bohrmann et al., 2003; Nikishin et al., 2003). By contrast, in the northern Gulf of Mexico (Green Canyon Bush Hill and 415 East) and on the Nile deep-sea fan (Giza and North Alex MVs) in the eastern Mediterranean Sea (Roberts and Carney, 1997; Loncke et al., 2004, 2006), fluid seepage and mud volcanism are caused by thin-skinned tectonic processes. In these areas, huge sediment accumulation rates and actively moving salt bodies in the subsurface create faults along which fluids, gas and mud are transported to the seafloor. In the Gulf of Cadiz, mud volcanism and related phenomena are concentrated along deeply cutting thrust and strike-slip faults that are associated with the boundary between the African and Eurasian plates (Pinheiro et al., 2005; Medialdea et al., 2009). In a recent study, Scholz et al. (2009) investigated five MVs located on an E–W transect across the Gulf of Cadiz (map 3 in Fig. 1). Deep-sourced pore fluids from this transect reflect the transition from continental-sedimentary to oceanic-crustal fluid sources. Scholz et al. (2009) inferred from Sr and Li isotope systematics that deep-seated faults serve as conduits for fluids originating in the underlying oceanic basement and drew parallels to ridge-flank hydrothermal systems.

2.2. Diagenetic characterization of pore fluids

Deeply buried sediments on continental margins are strongly reducing environments. Accordingly, deep-sourced

pore fluids are, in most cases, devoid of SO_4^{2-} but strongly enriched in reduced components such as NH_4^+, I^- and CH_4 (e.g., Aloisi et al., 2004; Wallmann et al., 2006a; Fehn et al., 2007; Gieskes and Mahn, 2007). Many of the pore fluids investigated here have lower salinities than normal seawater. Fresh water contributions from dissociating gas hydrates or groundwater aquifers have largely been ruled out based on the oxygen and hydrogen isotope composition of the pore fluids (e.g., Dählmann and De Lange, 2003; Hensen et al., 2007). Instead, dehydration of clay minerals in the deep subsurface is commonly regarded as the major reason for pore water freshening (Kastner et al., 1991; Moore and Vrolijk, 1992; Dählmann and De Lange, 2003; Hensen et al., 2004, 2007). Clay mineral dehydration processes such as the conversion of smectite to illite chiefly occur at temperatures between 60 and 150 °C and are accompanied by K consumption and the release of Na, B and Li into the ambient pore water (Ishikawa and Nakamura, 1993; Środoń, 1999; Chan and Kastner, 2000). The release of mobile cations from sediments continues at temperatures beyond the typical range for clay diagenesis leading to very high B and Li concentrations in décollement fluids at subduction zones and in fluids of sediment-hosted hydrothermal systems (Butterfield et al., 1994; You et al., 1996; James et al., 1999; Kastner and Rudnicki, 2004). In some cases (e.g., Green Canyon 415 East in the Gulf of Mexico, Napoli Dome in the Mediterranean Sea, Dvurechenskii MV in the Black Sea), the clay mineral diagenetic signal of pore water dilution is overprinted by admixing of evaporated seawater or by dissolution of evaporite minerals (e.g., Dählmann and De Lange, 2003; Aloisi et al., 2004; Reitz et al., 2007).

In order to investigate the above-described processes independently from each other, 'reference' fluids with a less complex geochemical evolution have been included in this study. Shallow pore waters from the Nile deep-sea fan and the eastern Black Sea show downcore decreasing Li concentrations indicating Li uptake by sediments during early diagenesis (Zhang et al., 1998; James and Palmer, 2000). Lithium-rich pore fluids from sediments in the Okinawa Trough hydrothermal system (Fig. 1) are formed through interaction of seawater with andesitic volcanic rocks and terrigenous sediments at temperatures above 300 °C (Glasby and Notsu, 2003; Konno et al., 2006). Brine samples have been obtained from two evolutionarily distinct brine basins in the eastern Mediterranean Sea (map 4 in Fig. 1). While Bannock brine has evolved through 12-fold evaporation of seawater and subsequent burial (Vengosh et al., 1998), Discovery brine has formed through dissolution of late-stage evaporite minerals (mainly bischofite, $MgCl_2{\cdot}6H_2O$) by sediment pore waters (Wallmann et al., 1997).

3. METHODS

3.1. Sediment sampling and pore water recovery

Pore water samples for this study were obtained on several cruises using piston and gravity corers equipped with PVC or tube foil liners, multi or mini corers and ROV-guided push cores (Table 1). Brine samples were collected with Niskin bottles mounted on a CTD/rosette (De Lange et al., 1990). Upon recovery, core liners were sectioned, sealed and transferred into a cooled laboratory to ensure subsampling under in situ (i.e., seafloor) temperature. Subsamples were taken within regular distance from the lengthwise-cut sediment cores. Multi and mini cores were stepwise extruded from the liners and cut into 1–3 cm thick slices. Pore water recovery was done by pressure filtration (argon gas at 2–5 bar) or by centrifuging (4000 rpm for 20 min). Pore waters were filtered through 0.2 μm cellulose-acetate membrane filters and then divided into aliquots for shipboard and shore-based analyses. Aliquots for cation analyses were acidified (HCl or HNO_3, suprapur) to prevent any mineral precipitation or adsorption. For the same reason, brine samples were additionally diluted 1:3 with bi-distilled water. Pore water and brine samples were stored cooled until further processing on land.

3.2. Laboratory analyses

Chlorinity measurements were carried out on-board by Ion Chromatography (761 IC-Compact, Metrohm) or titration with 0.01N $AgNO_3$ (Grasshoff et al., 2002). Lithium was analyzed by Inductively Coupled Plasma Optical Emission Spectrometry (ICP-OES, JY 170 Ultrace, Jobin Yvon). The analytical precision based on repeated analysis of IAPSO seawater standard is <1% for Cl and <5% for Li. Further information about these routine methods may be obtained from the IFM-GEOMAR web page.

Lithium isotope analyses were carried out by Multi Collector Inductively Coupled Plasma Mass Spectrometry (MC ICP-MS, NEPTUNE, ThermoFisher Scientific) after chromatographical Li separation following a modified protocol after Tomascak et al. (1999). For ion exchange chromatography, a sample aliquot containing 0.5 μg Li was evaporated and re-dissolved in 1N HNO_3 and 80% methanol. Samples with a high molar Na/Li ratio ($>\sim 2 \times 10^5$) were subjected to a second or third chromatographical step using 0.5N HCl and 80% methanol as solvent (modified after Jeffcoate et al., 2004). The Li recovery after sample purification was typically >99.9%. The Li standard NIST SRM 8545 (L-SVEC) and seawater were repeatedly included in the chromatographic separation to check the accuracy of the procedure. The resulting Li isotope values are reported relative to the standard NIST SRM 8545 according to $\delta^7Li = (({}^7Li/{}^6Li)_{sample}/({}^7Li/{}^6Li)_{standard} - 1) \times 1000$. Repeated analysis of seawater during this study yielded a δ^7Li of $30.9 \pm 0.3‰$ (2σ, $n = 9$). Further details on the ion chromatographic and mass spectrometric procedures are given in Wunder et al. (2006, 2007).

Strontium isotope ratios were determined by Thermal Ionization Mass Spectrometry (TIMS, TRITON, ThermoFisher Scientific) after chemical separation via cation exchange chromatography using a Sr-specific resin (Eichrom). All isotope ratios were internally normalized to an $^{86}Sr/^{88}Sr$ ratio of 0.1194. Repeated analysis of the standard NIST SRM 987 over the course of this study yielded an average value of 0.710220 ± 17 (2σ, $n = 12$). For comparison with literature values all $^{87}Sr/^{86}Sr$ were normalized to a value of 0.710248 for the NIST SRM 987.

3.3. Transport-reaction modeling

A one-dimensional, numerical transport-reaction model was developed to simulate Li isotope fractionation during upward advection of pore fluids. Partial differential equations for solutes follow the classical approach of Berner (1980):

$$\phi \cdot \frac{\partial [C]}{\partial t} = \frac{\partial \left(\phi \cdot D_S \cdot \frac{\partial [C]}{\partial x} \right)}{\partial x} - \frac{\partial (\phi \cdot v \cdot [C])}{\partial x} + \phi \cdot R \qquad (1)$$

where $[C]$ is the concentration of dissolved species in pore water, x is depth, t is time, ϕ is porosity, D_S is the molecular diffusion coefficient in sediments, v is the vertical advection velocity of the pore water and R defines all reactions occurring in the simulated sediment domain. The model calculates the concentration-depth profiles of three dissolved species (total dissolved Li, ^{7}Li and ^{6}Li) considering the decrease in porosity with sediment depth, molecular diffusion, advective transport of solutes via sediment burial, steady-state compaction and pressure-driven flow as well as the temperature-dependent precipitation of Li and the related isotope fractionation.

Sediment porosity decreases with depth due to sediment compaction. Assuming steady-state compaction, the profile can be approximated by:

$$\phi(x) = (\phi_{TOP} - \phi_{BOT}) \cdot \exp(-const \cdot x) + \phi_{BOT} \qquad (2)$$

where ϕ_{BOT} and ϕ_{TOP} are the porosity at the lower and upper boundary and *const* is the attenuation coefficient for the exponential decrease of porosity with depth. The burial velocity of solids is expressed as steady-state compaction with:

$$\omega(x) = \frac{1 - \phi_{BOT}}{1 - \phi(x)} \omega_{BOT} \qquad (3)$$

where $\omega(x)$ represents the depth-dependent burial velocity and ω_{BOT} is the sediment burial velocity at the base of the model domain. The upward directed pore water velocity through sediments is composed of the downward burial

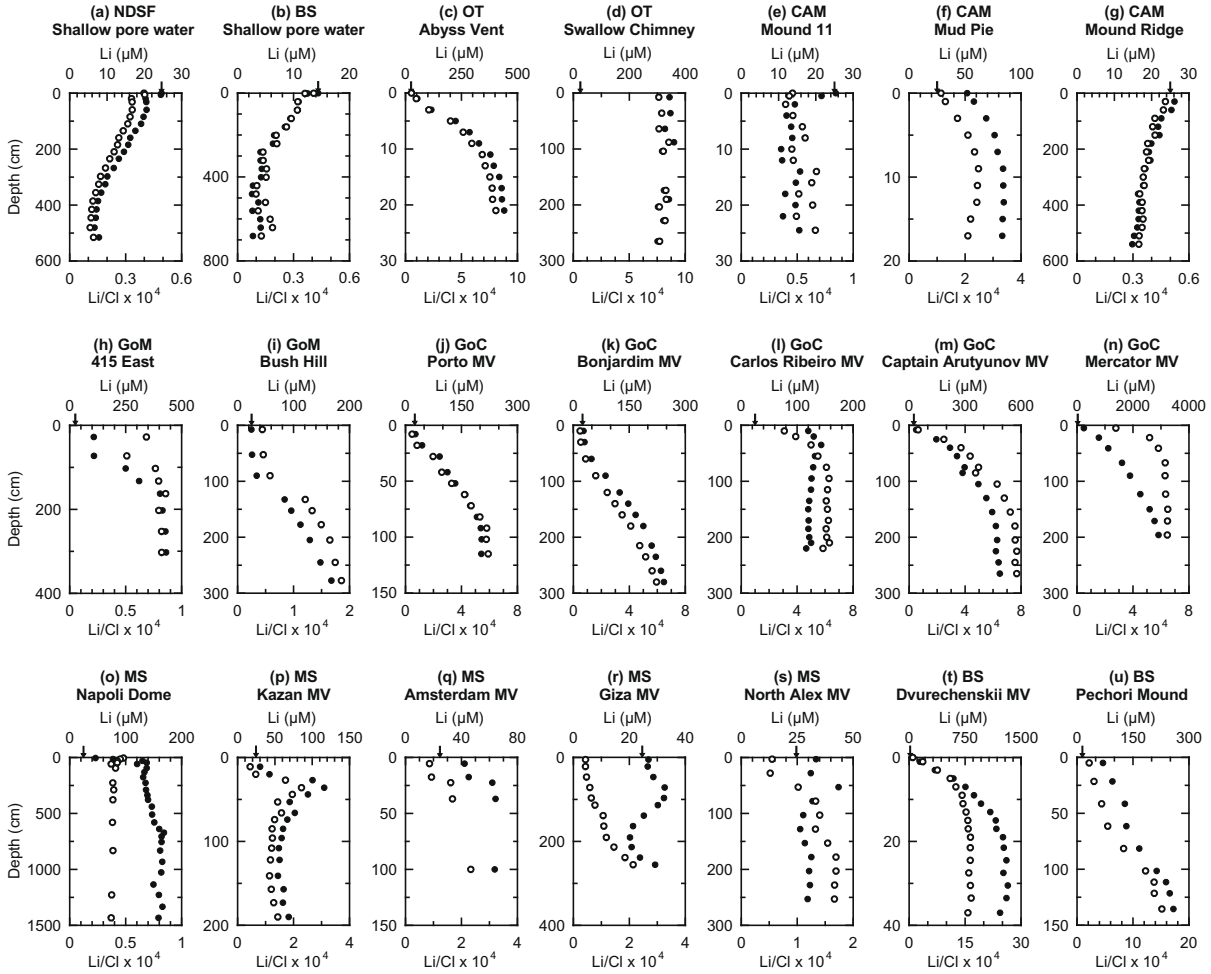

Fig. 2. Pore water profiles of Li concentration (black circles) and Li/Cl ratio (open circles) for all studied sediment cores. Arrows on upper axis indicate the normal seawater Li concentration (26 μM). Pore water profiles of different cores from the same site are similar to each other. Therefore, only one profile per site is shown ((l) 174-GC9, (n) 239-GC20, (p) AX18GC1, (q) AX02AP2, (r) GC5, (t) GeoB11977). Abbreviations for study areas are as follows: NDSF, Nile deep-sea fan; BS, Black Sea; OT, Okinawa Trough; CAM, Central American margin; GoM, Gulf of Mexico; GoC, Gulf of Cadiz; MS, Mediterranean Sea.

Table 2
Pore water and bottom water (BW) data for Cl, Li, δ^7Li and $^{87}Sr/^{86}Sr$.

Area	Location	Core	Depth (cm)	Cl (mM)	Li (μM)	δ^7Li (‰)	$^{87}Sr/^{86}Sr$
Reference sites							
Gulf of Cadiz		139-MUC2	BW	559	24.0	30.9	0.709179
Nile deep-sea fan		MUC28	BW	618	24.6	30.9	0.709200
		GC2	109.5	615	19.1	29.1	
			297.5	610	10.1	30.9	0.709130[d]
			415.5	609	7.18	29.6	0.709100[d]
Black Sea		GeoB11905	1.0	353	14.4	32.3	0.709136[d]
		GeoB11974	301.5	300	4.1	31.9	
Okinawa Trough	Abyss Vent	MUC28	21.0	546	204	5.8	0.709323
		44PC33	21.0	553	441	2.7	0.709483
	Swallow Chimney	34GC1	36.0	441	347	1.1	0.709788
			265.0	392	301	−0.7	0.709829
Mediterranean Sea	Discovery brine	PP28CT[c]	3672.0	9550	310	25.0	
			3677.0	9550	310	25.1	0.708961
			3672.0	9560	320	25.0	
	Bannock brine	PP09CT[c]	I-3460	5300	270	24.5	
			I-3505	5320	280	24.8	0.708650
			II-3612	5350	300	24.3	0.708629
Seep sites							
Central American margin	Mound 11	TVMUC127	19.0	230	13.2	29.6	
			23.5	230	13.4	29.9	0.708699
	Mud Pie	108/78/27	9.0	339	83.9	23.7	0.707320
			11.0	345	84.1	24.4	
	Mound Ridge	GC219	510.0	445	11.2	27.6	
			540.0	424	11.0	27.2	0.709126
Gulf of Mexico[a]	Green Canyon 415 East	TGC3	202.5	5200	414	45.7	0.708629
			252.5	5210	428	45.4	
			302.5	5240	430	44.8	0.708625
			302.5-r			44.7	
	Green Canyon Bush Hill	GC8	245.0	849	148	23.3	
			277.5	903	168	23.6	0.708663
			18.0	539	44	24.2	0.708676
			62.0	380	160	15.3	0.707668
Gulf of Cadiz[b]	Porto MV	143-GC3	102.0	353	204	12.1	0.707534
			115.0	344	203	12.2	0.707536
	Bonjardim MV	130-GC1	160.0	480	167	19.6	0.708694
			180.0	458	188	19.5	
	Carlos Ribeiro MV	154GC5	200.0	199	122	19.7	0.708208
			220.0	199	116	20.0	0.708208
	Captain Arutyunov MV	174-GC9	245.0	633	479	16.3	0.709922
		205-GC13	270.0	623	503	17.2	0.709910[d]
	Mercator MV	239-GC20	171.0	4280	2770	12.5	0.710626
			196.0	4510	2910	12.5	0.710613
		263-GC28	116.0	5080	3270	11.9	0.710628
Mediterranean Sea	Napoli Dome	KC11	832.0	4190	162	17.1	
			1228.0	4190	159	17.2	
			1433.0	4190	159	17.7	0.708407
	Kazan MV	AX18GC1	46.0	254	57.3	16.6	
			62.5	198	68.0	16.6	0.707938
		MS07GT	11.0	672	30.1	30.9	
			36.0	508	116	14.7	0.707932
			173.0	470	60.7	22.7	
	Amsterdam MV	AX02AP2	37.0	383	64.4	22.0	
			100.0	273	63.8	20.6	
		AX02AP3	55.0	299	66.8	22.2	
			76.0	246	65.6	22.1	0.708550
	Giza MV	GC5	96.5	506	32.4	23.0	
			190.5	172	20.2	22.8	
			255.5	137	29.2	20.7	0.707820
		GC34	219.5	165	29.1	21.9	0.707642[d]

Table 2 (*continued*)

Area	Location	Core	Depth (cm)	Cl (mM)	Li (μM)	δ^7Li (‰)	$^{87}Sr/^{86}Sr$
	North Alex MV	GC100	53.0	427	43.5	20.6	0.706590[d]
			128.0	199	26.3	21.9	0.706587[d]
			203.0	179	30.3	19.6	
Black Sea	Dvurechenskii MV	GeoB11977	30.5	805	1322	7.5	0.708310
			33.5	784	1300	7.7	
		GeoB11978	30.5	786	1240	7.5	
			33.5	789	1230	7.6	
	Pechori Mound	GeoB11955	121.5	180	249	14.0	0.707890
			135.5	170	258	14.1	

[a] $^{87}Sr/^{86}Sr$ data from Reitz et al. (2007).
[b] Data from Scholz et al. (2009).
[c] Water depth in meter below sea surface.
[d] Measured on samples from neighboring depth interval.

component modified by compaction and the upward fluid advection:

$$v(x) = \frac{\omega_{BOT} \cdot \phi_{BOT} - v_{TOP} \cdot \phi_{TOP}}{\phi(x)} \quad (4)$$

where $v(x)$ represents the depth-dependent fluid velocity and v_{TOP} is the upward fluid advection velocity at the sediment surface.

Temperature-dependent molecular diffusion coefficients of Li were calculated after Boudreau (1997) and corrected for tortuosity using the following relationship (Boudreau, 1996):

$$D_S(x) = \frac{D_M(x)}{1 - \ln(\phi(x))^2} \quad (5)$$

where D_M is the molecular diffusion coefficient in seawater. The same value of D_M was used for both Li isotopes. Temperature variations from bottom water to the lower boundary of the simulated sediment column were also considered in a depth-dependency of D_M.

The rate law for Li precipitation and isotope fractionation as well as the boundary conditions and fitting parameters for the model runs are specified in Section 5.2. The model was run to steady state from arbitrary initial conditions. Finite difference techniques (the method-of-lines code) were applied to solve the partial differential equations (PDEs). A set of three PDEs (one for each species) is converted into 200 ordinary differential equations (ODE) giving the temporal change of species concentration at each depth interval. The ODE system was set up on an uneven grid with higher resolution at the surface and solved using the NDSolve object of MATHEMATICA Version 7.0 (cf. Hensen and Wallmann, 2005; Wallmann et al., 2006b, 2008).

4. RESULTS

Depth profiles for dissolved Li concentrations and molar Li/Cl ratios are plotted in Fig. 2. Ratios of Li/Cl highlight deviations from the general salinity trend, i.e., denote consumption or release of Li during chemical reactions. A compilation of δ^7Li, $^{87}Sr/^{86}Sr$ as well as Cl and Li concentration data is given in Table 2. Lithium isotope data of MVs in the Gulf of Cadiz have previously been published by Scholz et al. (2009).

Pore fluids from hemipelagic sites are characterized by downcore decreasing Li/Cl ratios but seawater-like δ^7Li values (Fig. 2a and b, Table 2). Hydrothermal fluids from the Okinawa Trough are considerably enriched in Li and show comparably light δ^7Li values between −0.7‰ and +5.8‰. The δ^7Li of brine samples varies over a narrow range from +24.3‰ to +25.1‰.

Most pore water profiles of cold seeps display a mixing relationship between bottom water concentrations at the top and an almost uniform concentration in the lower core section. In accordance with previous studies (e.g., Hensen et al., 2007; Scholz et al., 2009), pore waters from below the mixing zone between seawater and upwelling fluid will be referred to as 'deep fluid' in the following sections. Most deep fluids display Cl concentrations below local bottom water values (Table 2), which has been ascribed to dilution with freshwater derived from clay mineral dehydration (cf. Dählmann and De Lange, 2003; Hensen et al., 2004, 2007; Haese et al., 2006). Chloride concentrations above seawater at a few locations have been attributed to dissolution of evaporite minerals (e.g., Green Canyon 415 East, Reitz et al., 2007; Mercator MV, Scholz et al., 2009; Napoli Dome, Dählmann and De Lange, 2003; Dvurechenskii MV, Aloisi et al., 2004). Lithium enrichments above local bottom water values or elevated Li/Cl ratios in most cores indicate release of Li from sediments or rocks during diagenetic processes. Exceptions are two sites at the Central American margin (Mound 11, Mound Ridge; Fig. 2e and g) where Li concentrations and Li/Cl ratios are constant or even decrease with depth. The δ^7Li of deep fluids varies over a broad range from +7.5‰ at Dvurechenskii MV in the Black Sea to +45.7‰ at Green Canyon 415 East in the Gulf of Mexico (Table 2).

5. DISCUSSION

5.1. Controls on the lithium isotope composition of marine pore fluids

Most of the cold seep fluids investigated here originate from much greater sediment depths than may be reached by conventional coring techniques. A general concept of the controls on their Li isotope signature may be obtained by comparing the presented results with reference data that

have been collected in related marine settings. Fig. 3a presents a compilation of Li concentration and δ^7Li data of vent and pore fluids from normal ridge-crest and sediment-hosted hydrothermal systems and of deep-seated interstitial fluids from the ODP (see Electronic Annex for table of data and references). The interstitial fluids are grouped into low-temperature and high-temperature diagenetic pore fluids according to the original data interpretation. Processes referred to as low-temperature diagenesis are cation exchange and Li uptake by authigenic clay minerals in shallow sediments (e.g., Zhang et al., 1998; James and Palmer, 2000). In contrast, Li release from primary minerals at elevated temperatures (>~50 °C) (You et al., 1995; Chan and Kastner, 2000) coupled to uptake of Li by secondary minerals (James and Palmer, 2000) represents the major high-temperature diagenetic process. The reference data plotted in Fig. 3a show a pronounced negative correlation between δ^7Li and Li concentration. This general trend may be expressed by the following empirical relationship:

$$\delta^7\mathrm{Li} = -6.0(\pm 0.3)\cdot \ln[\mathrm{Li}] + 51(\pm 1.2) \quad (6)$$

The different fluid types define distinct Li and δ^7Li ranges which are ordered according to increasing reaction temperature within the respective geological systems (low-temperature diagenetic – high-temperature diagenetic – hydrothermal). This general sequence is also confirmed by the new reference data of pore waters from shallow, hemipelagic sediments and hydrothermal pore fluids from the Okinawa Trough (Fig. 3a).

5.1.1. Hydrothermal fluids

Fluids from hydrothermal systems plot close to or within the average range of δ^7Li values reported for MORB and detrital sediment, respectively (bars on right-hand side of Fig. 3a). A straightforward explanation for this isotopic composition could be simple leaching of Li from minerals without any further reaction. The δ^7Li of a fluid (subscript *F*) resulting from binary mixing between

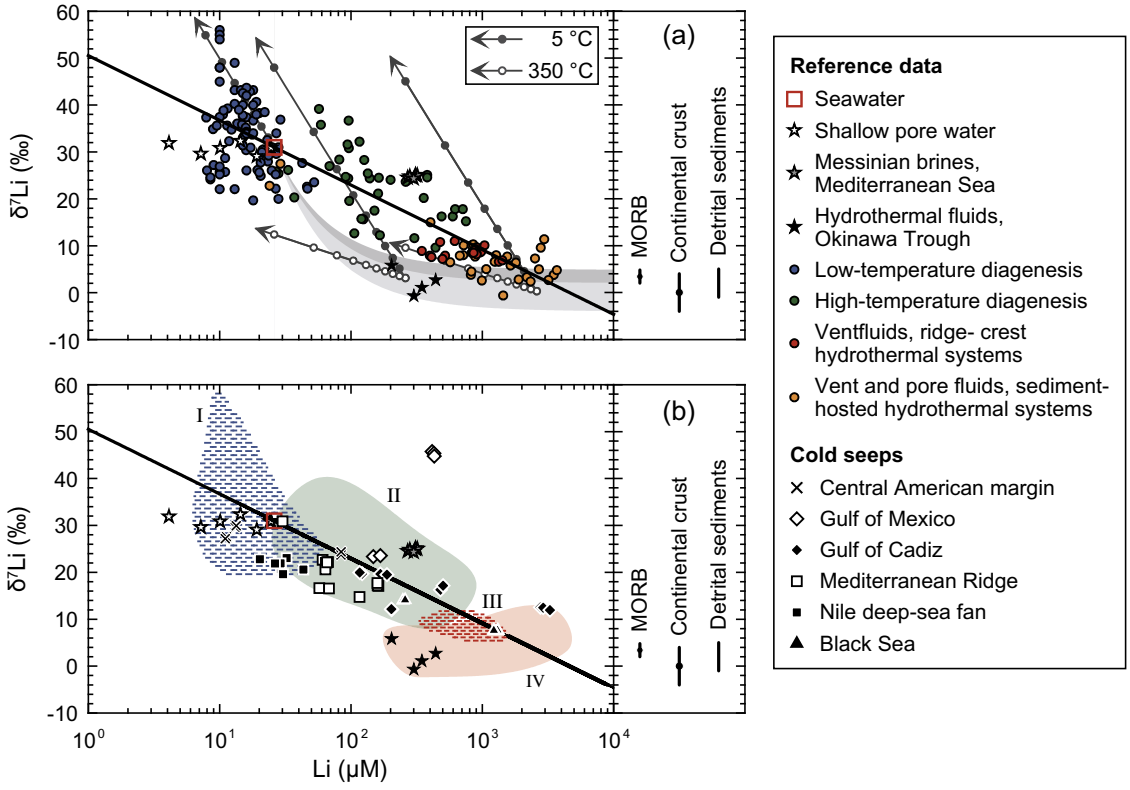

Fig. 3. Plots of δ^7Li versus Li concentration for reference data (a) and cold seep fluids (b). Note logarithmic scale of *x*-axis. Reference data are grouped into low-temperature diagenetic fluids, high-temperature diagenetic fluids, vent fluids from ridge-crest hydrothermal systems and vent and pore fluids from sediment-hosted hydrothermal systems (Chan et al., 1993, 1994; You et al., 1995, 2003; Zhang et al., 1998; James et al., 1999; Chan and Kastner, 2000; James and Palmer, 2000; Foustoukos et al., 2004). A table including all literature data is given in the Electronic Annex. Vertical bars in the inlet on the right-hand side depict the average isotopic composition of MORB (Tomascak et al., 2008), upper continental crust (Teng et al., 2004) and detrital marine sediments (Chan et al., 2006). Thick black lines in both diagrams represent the logarithmic regression through all reference data ($\delta^7\mathrm{Li} = -6.0(\pm 0.3)\cdot \ln[\mathrm{Li}] + 51(\pm 1.2)$; $R^2 = 0.76$). Shaded arrays in (a) indicate mixing between seawater Li and Li from fresh MORB (upper array) and the upper continental crust (lower array). The gray lines in (a) have been calculated using a Rayleigh fractionation model in order to exemplify the evolution of pore fluids during progressive Li uptake by authigenic clay minerals at 5 and 350 °C. Nodes on the gray lines depict the fraction of initial Li (26, 260 and 2600 μM) remaining in the fluid ($[\mathrm{Li}]_{PF}/[\mathrm{Li}]_F = 1.0$–$0.1$). Colored domains in (b) encompass the Li concentration and δ^7Li ranges of reference fluid types: I, low-temperature diagenesis; II, high-temperature diagenesis; III, ridge-crest hydrothermal systems; IV, sediment-hosted hydrothermal systems. See text for further explanation.

seawater Li (subscript *SW*) and solid phase Li (subscript *SP*) can be written as follows:

$$\delta^7Li_F = \frac{[Li]_{SW}}{[Li]_F} \cdot \delta^7Li_{SW} + \frac{[Li]_{SP}}{[Li]_F} \cdot \delta^7Li_{SP} \quad (7)$$

The shaded mixing arrays in Fig. 3 were calculated applying a δ^7Li_{SW} of +31‰ (Millot et al., 2004) and recently reported δ^7Li ranges reported for MORB (+3.4 ± 1.4‰; Tomascak et al., 2008) and for upper continental crust (0.0 ± 1.4‰; Teng et al., 2004). The average δ^7Li of the upper continental crust by Teng et al. (2004) is based on a variety of shales, loess, granites and other crustal composites. This average value is considered the best estimate of the isotopic composition of terrigenous sediments prior to interaction with fluids in diagenetic or nearshore hydrothermal environments.

Some of the fluids from sediment-hosted hydrothermal systems (e.g., those from the Okinawa Trough) plot within the mixing array between seawater and the upper continental crust (Fig. 3a) suggesting that their δ^7Li is dominated by simple Li release from minerals. Most of the hydrothermal fluids, however, show a distinct offset from the mixing arrays towards heavier δ^7Li values. Since isotope fractionation during incongruent mineral dissolution was found to be negligible (Pistiner and Henderson, 2003), this offset is commonly attributed to subsequent incorporation of isotopically light Li into secondary clay minerals (e.g., Chan et al., 1993; James et al., 1999). The average δ^7Li of hydrothermal fluids is +8.6 ± 1.3‰ for sediment-free systems and +5.7 ± 3.1‰ for sediment-hosted systems (the shallowest three samples from ODP Site 1038 in the Escanaba Trough have not been considered in this calculation because of their disproportionally high content of pristine seawater; cf. James et al., 1999). Interestingly, the isotopic offset between fluids from sediment-free systems and MORB (5.2‰) and fluids from sediment-hosted systems and the upper continental crust (5.7‰) are in remarkable agreement. Differences in δ^7Li between the two fluid types reflect the isotopic difference between the upper continental crust and the upper mantle, which, in turn, has been attributed to preferential retention of the light Li isotope during weathering of crustal material (Teng et al., 2004). Preservation of this primary signal in hydrothermal fluids is remarkable, considering the extent of alteration occurring subsequently to the release of Li in the hydrothermal reaction zone. Higher Li concentrations in fluids from sediment-hosted hydrothermal systems are attributed to higher Li concentrations in clastic marine sediment with respect to MORB (Chan et al., 2006; Tomascak et al., 2008) and, in addition, to the higher extraction efficiency of Li from sediments (James et al., 2003).

5.1.2. Sediment interstitial fluids

In conformity with pore fluids of sediment-hosted hydrothermal systems, high-temperature diagenetic pore fluids are affected by Li release from sediments. Because of the lower temperatures prevailing in diagenetic environments, however, less Li is extracted from primary minerals and relatively more Li is sequestered by secondary minerals (Berger et al., 1988; James and Palmer, 2000; James et al., 2003). As a consequence, the pore fluids' Li concentrations are lower and their δ^7Li values are heavier compared to hydrothermal fluids (Fig. 3a).

Depending on factors such as concentration-depth gradient, pore pressure and heat flow, Li in interstitial fluids undergoes advective and diffusive transport. In either case, pore water Li is unlikely to remain in contact with alteration products. As a consequence, the δ^7Li of the remaining pore fluid (subscript PF) can be approximated by a Rayleigh-type equation:

$$\delta^7Li_{PF} = \left(\frac{[Li]_{PF}}{[Li]_F}\right)^{\alpha-1} \cdot (\delta^7Li_F + 10^3) - 10^3 \quad (8)$$

The Li concentration and δ^7Li evolution of fluids during progressive Li loss to authigenic clay minerals is illustrated in Fig. 3a. Starting values lie on the mixing line between seawater Li and Li derived from sediments at 100-fold, 10-fold and normal seawater concentration. Fractionation factors between authigenic clay minerals and pore fluids for low and high temperature end members were taken from Chan et al. (1994): $\alpha_{mineral-fluid} = 0.981$ for 5 °C and $\alpha_{mineral-fluid} = 0.996$ for 350 °C.

Most pore water Li data that have been published so far for diagenetic environments may be explained with a combination of mixing with Li from sediments or rocks (see Section 5.1.1) and Raleigh fractionation during formation of secondary minerals (Fig. 3b). The increasing distance of the general trend from the mixing arrays towards lower Li concentrations reflects the enhanced isotope fractionation at lower temperatures (Chan et al., 1994). Most fluids from low-temperature diagenetic environments are characterized by lower Li concentrations than seawater. Many of these fluids display heavier δ^7Li values than seawater and plot close to the Rayleigh distillation line corresponding to Li uptake by secondary minerals at 5 °C (Fig. 3a). Other low-temperature diagenetic fluids, however, show δ^7Li values equal to or even below seawater. Likewise, new Li data of pore waters from surficial hemipelagic sediments on the Nile deep-sea fan and in the eastern Black Sea show seawater-like δ^7Li values throughout the core (Table 2) although downward decreasing Li concentrations within the upper four meters indicate shallow Li removal (Fig. 2a and b). This combination of δ^7Li and Li concentration cannot be produced through isotope fractionation during incorporation of seawater Li into secondary minerals at low temperature. Instead, another Li-consuming process, involving less or no isotope fractionation, has to be considered.

In the crystal lattice of clay minerals, Li either replaces Mg in the structural, octahedral sites or it occupies the interlayers as an adsorbed cation. While structural incorporation produces a significant isotope fractionation, this is not necessarily the case for Li adsorption (Vigier et al., 2008). For instance, sorption experiments with vermiculite and kaolinite resulted in a significant Li isotope fractionation ($\alpha_{mineral-fluid}$ up to 0.971; Zhang et al., 1998). By contrast, Pistiner and Henderson (2003) and Vigier et al. (2008) observed no isotope fractionation during Li adsorption onto smectite. Smectite is the predominant clay mineral on the Nile deep-sea fan and in the eastern Black Sea (Venkatarathnam and Ryan, 1971; Stoffers and Müller,

1978). Accordingly, the downcore Li decrease in pore water at these sites is attributed to adsorption rather than structural incorporation. The large scattering of the low-temperature diagenetic fluids around seawater values suggests that adsorption onto smectite, or other mechanisms involving no or little isotope fractionation, play an important role in shallow marine sediments.

5.1.3. Cold seep fluids

The overall pattern of processes identified in the previous sections may be used as a general frame of reference for Li isotope exchange between fluids and silicate minerals in marine systems. Comparing signatures of the cold seep fluids with that reference frame is anticipated to reveal information about their origin and diagenetic evolution.

Fig. 3b shows the Li concentration and δ^7Li data of deep fluids from cold seeps along with the compositional ranges of reference fluids (cf. Fig. 3a). Most of the cold seep fluids plot within the domain characteristic for high-temperature diagenetic environments. Many of the reference samples in this domain are décollement fluids whose Li isotopic composition has been explained with sediment dehydration reactions deep within subduction zones. Laboratory experiments conducted by Williams and Hervig (2005) revealed extensive uptake of isotopically light Li from solution during illitization of smectite. Release of Li from sediments at temperatures >60 °C and incorporation into authigenic smectite–illite is in excellent agreement with the ubiquitous diagenetic signal of pore water freshening and other indicators for high-temperature fluid/sediment interactions at all seep locations investigated (Table 2; Dählmann and De Lange, 2003; Aloisi et al., 2004; Hensen et al., 2004, 2007; Haese et al., 2006; Reitz et al., 2007). However, some of the cold seep fluids plot within other domains (e.g., hydrothermal or low-temperature diagenetic) suggesting a differing or more diverse combination of processes or influencing factors.

Pore fluids of two seep locations on the Central American margin, Mound 11 and Mound Ridge, display comparably heavy isotopic compositions close to seawater. At these sites, little downcore deviation from the Li/Cl ratio of seawater indicates that Li has not been involved in chemical reactions to a significant extent (Fig. 2e and g).

Two seep sites, Dvurechenskii MV in the Black Sea and Mercator MV in the Gulf of Cadiz, plot within the domain of sediment-hosted hydrothermal systems. The fluid composition of Dvurechenskii MV is in excellent agreement with the empirical relationship between δ^7Li and Li concentration in marine systems (Fig. 3b). Therefore, it is reasonable to anticipate fluid-sediment interactions at temperatures beyond the range typical for clay mineral diagenesis (>150 °C) at this location. In case of Mercator MV, however, fluids have disproportionately high Li concentrations compared to their δ^7Li value (Fig. 3b). Scholz et al. (2009) attributed the exceptionally high Li content of deep-sourced pore fluids in the Gulf of Cadiz to the terrigenous/continental provenance of sediments in this area. Felsic continental rocks are moderately enriched in Li compared to mafic material (Wedepohl, 1978). Moreover, Li is retained in minerals during chemical weathering and additional Li is taken up during transport of eroded solids into the ocean (Rudnick et al., 2004; Kısakürek et al., 2005). As a result, terrigenous sediments and sedimentary rocks have very high Li concentrations, sometimes exceeding 100 mg kg^{-1} (Teng et al., 2004; Chan et al., 2006). The influence of the provenance and/or composition of marine sediments on the Li concentration of adjacent pore fluids is further illustrated in a plot of ^{87}Sr/^{86}Sr versus Li concentration in Fig. 4. All cold seep fluids which have undergone appreciable interaction with sediments or rocks show a positive correlation between ^{87}Sr/^{86}Sr and Li concentration. Pore fluids of Mercator MV, the shallowest seep site in the Gulf of Cadiz (map 3 in Fig. 1), have the most radiogenic ^{87}Sr/^{86}Sr ratios and the highest Li concentrations (Table 2). Accordingly, they are considered the terrigenous/continental deep fluid end member.

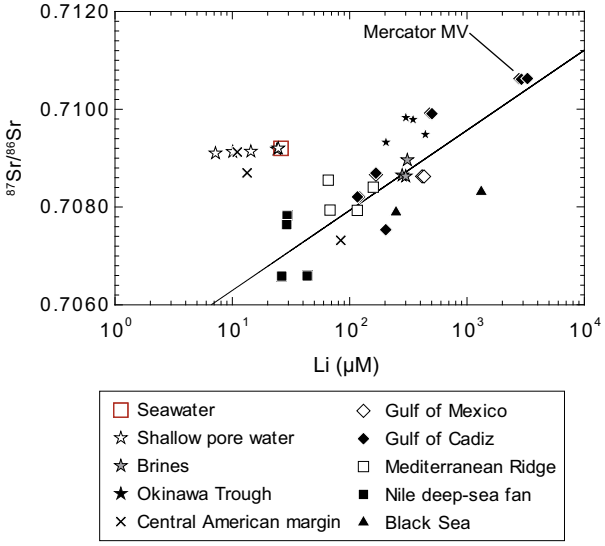

Fig. 4. Plot of ^{87}Sr/^{86}Sr versus Li concentration for cold seep fluids. Note logarithmic scale of *x*-axis. The black line represents a logarithmic regressions through the cold seep data ($R^2 = 0.72$; fluids of Mound 11 and Mound Ridge have been excluded since they show little evidence for exchange with sediments).

In contrast to that, pore fluids of Mud Pie on the Central American margin and seep locations on the Nile deep-sea fan display the least-radiogenic ^{87}Sr/^{86}Sr ratios and the lowest Li concentrations (Table 2, Fig. 4). Siliciclastic sediments in these areas are derived from Cenozoic, mostly mafic volcanic rocks in the Central American Arc (Kimura et al., 1997) and the Ethiopian highlands (Ryan et al., 1973; Foucault and Stanley, 1989), respectively. Because of the comparably low Li content of their catchment rocks (Wedepohl, 1978), rivers draining such volcanic terrains have lower Li concentrations in their bed load and suspended matter (<20 mg kg^{-1} in rivers on the Azores and Iceland; Pogge von Strandmann et al., 2008, 2010) than rivers draining continental rocks (up to several 100 mg kg^{-1} in Himalayan rivers; Kısakürek et al., 2005). As a consequence, young volcanogenic sediments on the Central American margin and the Nile deep-sea fan contain less leachable Li than the old and extensively weathered terrigenous sediments of the Gulf of Cadiz. Moreover, alteration

of labile volcanic minerals and ash particles to smectite and zeolites in the sediments may further deplete ambient pore fluids in Li (Kastner and Rudnicki, 2004). Therefore, non-radiogenic $^{87}Sr/^{86}Sr$ ratios are coupled to lower dissolved Li concentrations and comparably high δ^7Li values in these areas (Fig. 3b). Owing to intense alteration of volcanic matter, smectite is a major constituent of sediments on both the Nile deep-sea fan and the Central American margin (Venkatarathnam and Ryan, 1971; Spinelli and Underwood, 2004). It was shown in Section 5.1.2 that adsorption of Li onto smectite may remove a considerable portion of dissolved Li from pore water, without causing any isotope fractionation. Due to this process, seep fluids of the Nile deep-sea fan display disproportionally low Li concentrations compared to their δ^7Li values and plot in the transition area between the high-temperature and the low-temperature diagenetic domains in Fig. 3b. Smectite has the largest cation exchange capacity of the common clay minerals in marine sediments (Stumm and Morgan, 1995) and is most abundant on convergent margins and in other volcanogenic settings (Griffin et al., 1968). In addition to alteration of ash, Li adsorption is likely to limit pore water Li concentrations in such areas. As a consequence, seep fluids with the least-radiogenic $^{87}Sr/^{86}Sr$ ratios and low Li concentrations in Fig. 4 are considered the volcanogenic deep fluid end member.

Pore fluids of the cold seep Green Canyon 415 East in the Gulf of Mexico display particularly high Li concentrations and δ^7Li values beyond any of the reference domains (Fig. 3b). Comparison with the Rayleigh distillation lines in Fig. 3a demonstrates that near-complete scavenging of Li during transport at low temperature could have produced this fluid composition. Alternatively, anomalously high δ^7Li values and Li concentrations could be related to the strongly increased salinity of the fluids (Cl >5000 mM; Table 2), i.e., to fractionation mechanisms specifically related to brine formation.

5.1.4. Marine brines

Evaporite beds and local occurrences of evaporated and infiltrated seawater, also referred to as primary brines, are common features in deeply buried continental margin sediments. Interaction of pore fluids with evaporite minerals or mixing with a primary brine can lead to a significant alteration of the original diagenetic signal. Many deep-seated pore fluids reveal coinciding enrichments of Li, Cl and Na (e.g., Bernasconi, 1999; Aloisi et al., 2004; Reitz et al., 2007; Scholz et al., 2009). A systematic investigation of Li isotopes in hypersaline, sedimentary environments is therefore an important prerequisite to apply the general reference frame, outlined in previous sections, to these fluids.

Fig. 5a shows Na and Cl data for all cold seep fluids with elevated salinity as well as for the Discovery and Bannock brines. The evaporation pathway of seawater and a line denoting Na/Cl ratios of unity are shown for

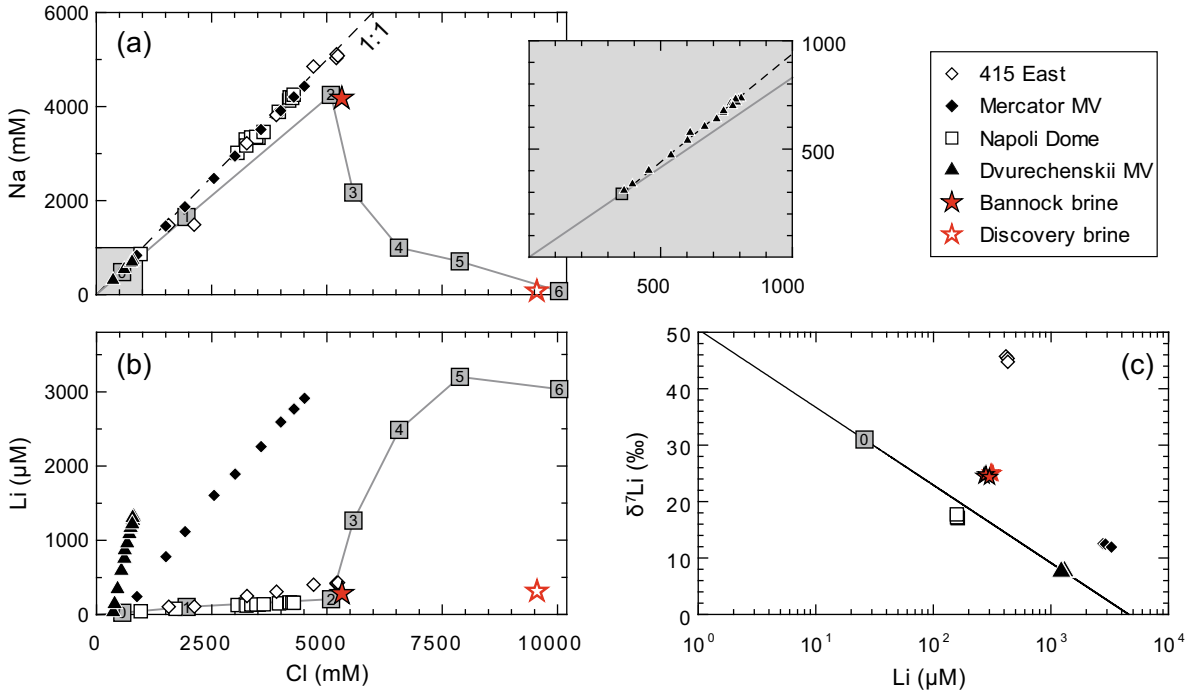

Fig. 5. Plots of Na versus Cl (a), Li versus Cl (b) and δ^7Li versus Li (c) for hypersaline cold seep fluids as well as the Bannock and Discovery brines. Pore water profiles of different cores from the same site resemble each other. Therefore, only one core per site is shown (cf. Fig. 2). Gray lines and squares in (a) and (b) depict the chemical evolution of seawater during progressive evaporation and precipitation of evaporite minerals: 0, seawater; 1, gypsum; 2, halite; 3, epsomite; 4, sylvite; 5, carnallite; 6, bischofite (from Fontes and Matray, 1993). The dashed line in (a) depicts Na/Cl ratios of unity. Due to the reduced salinity in the Black Sea, Na and Cl data of Dvurechenskii MV are shown in a separate plot with adapted scale. The black line in (c) represents the empirical relationship between δ^7Li value and Li concentration in marine systems (cf. Fig. 3a). Note logarithmic scale of *x*-axis in (c).

comparison. All hypersaline pore fluids contain equimolar proportions of Na and Cl which indicates that dissolution of halite (NaCl) is the most common reason for elevated pore water salinities at cold seeps. Proportions of Li to Cl, however, strongly diverge from each other (Fig. 5b) suggesting that the Li enrichments are not related to halite dissolution. This inference is corroborated by the chemical composition of Discovery brine which has evolved through dissolution of late-stage evaporite minerals (mainly bischofite; Wallmann et al., 1997). Although late-stage evaporite minerals are by far more enriched in Li than halite (Sonnenfeld, 1984), Li concentrations of the Discovery brine fail to reach those measured in the pore fluids.

Since Li contributions from evaporite minerals are minor, significant effects on the δ^7Li of pore fluids are only to be expected if the isotopic composition of the evaporite-derived Li strongly diverges from that of the fluids. The δ^7Li of pore fluids and brines is plotted versus Li concentrations in Fig. 5c. Most of the samples, including the Bannock and Discovery brines, plot close to the general relationship between δ^7Li and Li concentration in marine systems (cf. Fig. 3a). The isotopic compositions of the Bannock and Discovery brines are almost indistinguishable, although their chemical evolution is entirely different. This clearly shows that the offset in δ^7Li from seawater in both cases has not been produced during evaporation or precipitation of evaporite minerals. Two studies have addressed the Li isotopic composition of brines so far. Bottomley et al. (1999) analyzed brines of the Canadian Shield and inferred a marine origin based on δ^7Li values close to modern seawater. In contrast, Chan et al. (2002) found δ^7Li values lighter than seawater (δ^7Li: +18.2‰ to +27.0‰) in Messinian oil field brines in Israel and attributed this to Li release from ambient sediments. This explanation is somewhat problematic in the present case, since Li concentrations of the Bannock brine are in good agreement with its evolution through 12-fold evaporation of seawater (Cl = ~5300 mM; Table 2).

Another possible, but yet unexplored, reason for isotopic differences between brines and modern seawater are temporal changes in basin chemistry due to prolonged isolation from the global ocean. Müller and Mueller (1991) reported a shift of $^{87}Sr/^{86}Sr$ ratios below that of Messinian seawater in Mediterranean evaporites of upper Messinian age ($^{87}Sr/^{86}Sr$ decrease from 0.7089 to 0.7086). The authors attributed this trend to the increasing proportion of Sr derived from the Nile river ($^{87}Sr/^{86}Sr = 0.7076$; Müller and Mueller, 1991) in the isolated Mediterranean basin. In general, Li dissolved in river water has an isotopic composition intermediate between seawater and the catchment rocks (mean δ^7Li of major world rivers: +23.4‰; Huh et al., 1998). Consequently, a temporal shift towards less radiogenic $^{87}Sr/^{86}Sr$ ratios in the isolated Mediterranean basin should have been accompanied by a decrease in δ^7Li as well. The $^{87}Sr/^{86}Sr$ ratio of the Bannock brine is in agreement with the decreased Mediterranean seawater ratio during the late Messinian ($^{87}Sr/^{86}Sr = ~0.7086$; Table 2) and, thus, with an offset in δ^7Li from the world ocean. By contrast, the $^{87}Sr/^{86}Sr$ ratio of the Discovery brine is equal to the global Messinian ratio ($^{87}Sr/^{86}Sr = ~0.7089$; Table 2). Therefore, temporal changes in basin chemistry towards the upper Messinian could explain for differences in δ^7Li among the two brines (0.5‰ on average). The overall isotopic offset from global seawater ($\geqslant 6$‰), however, must be caused by a different mechanism.

The above discussion has demonstrated that the Li isotope signature of brines is entirely independent from the actual brine formation. Instead, isotopic exchange with ambient sediments during burial or upward transport must have transferred isotopically light Li into the saline solutions. The Li isotope signature resulting therefrom follows the empirical relationship between δ^7Li and Li concentration in marine systems (Fig. 5c). It is therefore deduced that Li isotope systematics of marine brines do not reveal fractionation mechanisms other than those observed in marine environments that have normal salinities.

5.2. Lithium isotope fractionation during fluid advection

Lithium isotope constraints on the origin and evolution of pore fluids from comparison with reference fluids are limited by the differing modes of transport in the respective geological systems. In bare ridge-crest and most sediment-hosted hydrothermal systems, fluids are rapidly transferred to the seafloor through vigorous convection within the oceanic crust or overlying sediments (Fisher, 2004). In non-advective interstitial waters of hemipelagic sediments, Li moves slowly along a concentration-depth gradient through molecular diffusion. In either case, most of the Li isotope fractionation recorded in the δ^7Li of fluids is likely to have occurred in a relatively narrow temperature range. This is an important prerequisite for the validity of the Rayleigh distillation approach outlined in Section 5.1.2. Compared to hydrothermal systems, fluid advection at cold seeps is much slower and subject to strong temporal fluctuations (e.g., Castrec et al., 1996; Haese et al., 2006; Hensen et al., 2007). Pore fluids leach Li from deeply buried sediments at a depth of several km below seafloor and at temperatures between 50 and ~200 °C. Because of low Darcy velocities, fluids may cool down during upward transport and Li exchange due to mineral authigenesis is likely to occur at multiple temperatures. Consequently, the accompanying isotope fractionation cannot be approximated with a single fractionation factor and the aforementioned Rayleigh approach is not applicable anymore.

In order to evaluate the influence of varying transport modes on the extent of Li isotope fractionation, we applied a transport-reaction model to simulate the ascent of deep-seated pore fluids to the seafloor. A similar approach has been adopted by James et al. (1999) to model Li isotope systematics of fluids in the Escanaba Trough sediment-hosted hydrothermal system. The height of the modeled sediment column and the boundary conditions were chosen to embrace as much of the heterogeneity encountered at the various seep and reference sites as possible. Although such a generalized model scenario cannot explain specific pore water profiles at single sites, it may well be used to retrace the major fractionation trends identified in Fig. 3. The adopted sediment thickness of 2 km represents an intermediate value between typical fluid mobilization depths at cold seeps (~2 to >5 km; Kopf, 2002) and basement depths at

sediment-hosted or ridge-flank hydrothermal systems (~0.1 to >1 km; e.g., Davis et al., 1997; Fouquet et al., 1998). The Li concentration and δ^7Li value at the upper boundary correspond to average seawater values. The δ^7Li value at the lower boundary has been calculated from the mixing relationship between seawater and continental crust (Eq. (7)) assuming a Li concentration hundred times that of seawater (i.e., 2600 μM). This concentration is in the upper range of values observed for cold seep and hydrothermal fluids (Fig. 3). Concentrations of ^{6}Li and ^{7}Li were calculated from δ^7Li values assuming a ^{7}Li/^{6}Li ratio of 12.02 for the NIST SRM 8545 (Flesch et al., 1973).

It is known from laboratory experiments that the Li distribution coefficient between secondary minerals and fluids increases exponentially with decreasing temperature (Berger et al., 1988). However, the actual amount of Li sequestered by different minerals at a given temperature turned out to be strongly variable (Berger et al., 1988). For the present transport-reaction model, we have to consider a wide variety of mineral assemblages. Moreover, the amount of secondary minerals formed at the various sites is essentially unknown. For that reason, the following function was applied as a first order rate law for Li removal into secondary minerals:

$$R_{\mathrm{Li}_{PPT}}(x,t) = k_{PPT} \cdot \exp(-0.5 \cdot T) \cdot [\mathrm{Li}]_{PF}(x,t) \quad (9)$$

In agreement with Berger et al. (1988), the amount of Li precipitated (subscript *PPT*) depends on the Li concentration in the fluid and increases exponentially with decreasing temperature (T). The coefficient in the exponent was determined by adjusting the model to the general relationship between Li concentration and δ^7Li depicted in Fig. 3. The rate constant for Li precipitation, k_{PPT}, characterizes the ability of different sediment types to form authigenic clay minerals. A k_{PPT} of 1×10^{-4} a^{-1} has proven to fit most of the variance in the data set. Temperature-dependent Li fractionation factors for Li uptake by authigenic minerals were calculated according to the empirical relationship by Chan et al. (1994) ($\alpha_{PPT\text{–}PF} = -1 \times 10^{-7} T^2 + 8 \cdot 10^{-5} T +$ 0.981; T in °C). The amount of ^{6}Li and ^{7}Li precipitated was obtained from the general equation defining the isotope fractionation factor:

$$\alpha_{PPT\text{–}PF} = \frac{\left[\frac{^7\mathrm{Li}}{^6\mathrm{Li}}\right]_{PPT}}{\left[\frac{^7\mathrm{Li}}{^6\mathrm{Li}}\right]_{PF}} = \frac{\frac{[^7\mathrm{Li}]_{PPT}}{[^6\mathrm{Li}]_{PPT}}}{\frac{[^7\mathrm{Li}]_{PF}}{[^6\mathrm{Li}]_{PF}}} \quad (10)$$

by substituting $[^7\mathrm{Li}]_{PPT}$ with $[\mathrm{Li}]_{PPT} - [^6\mathrm{Li}]_{PPT}$:

$$[^6\mathrm{Li}]_{PPT} = \frac{[\mathrm{Li}]_{PPT}}{\left(\alpha_{PPT\text{–}PF} \cdot \left[\frac{^7\mathrm{Li}}{^6\mathrm{Li}}\right]_{PF} + 1\right)} \quad (11)$$

Note that ongoing leaching of Li during transport is not considered in the model. All parameters used to produce the model curves are summarized in Table 3 and in the caption of Fig. 6.

Model scenarios 1–4 (lines in Figs. 6 and 7) simulate transport of deep-seated fluids through sediments at a common rate constant, k_{PPT}, but varying upward fluid advection rates. Fluid advection rates were chosen to represent regional averages for sedimentary settings that are influenced by fluid seepage (e.g., Davie and Buffett, 2003; Hensen and Wallmann, 2005). In the absence of active upward advection, most of the dissolved Li is rapidly precipitated and the model curve traverses the domain of low-temperature diagenetic pore fluids (curve 1; Fig. 6). Since much of the isotope fractionation in that scenario occurs in a narrow temperature range close to bottom water conditions, the resulting curve runs roughly parallel to the 5 °C-Rayleigh distillation line in Fig. 3a. At a low advection rate of 0.003 cm a^{-1}, the effects of sediment burial, compaction and active fluid flow cancel out each other. A linear concentration-depth gradient (curve 2; Fig. 7a) indicates that deep-sourced Li is transported upwards by molecular diffusion. Because of the slowness of this transport mechanism, however, intense precipitation of light Li prevents the deep-seated signal from reaching the sediment surface (Fig. 6). The model curve corresponding to a moderate advection rate of 0.03 cm a^{-1}

Table 3
Properties and boundary conditions applied in the numerical transport-reaction model.

Parameter	Value
Column length	2000 m
Temperature, sediment surface, T_{TOP}	5 °C
Temperature, lower boundary, T_{BOT}	65 °C
Porosity, sediment surface, ϕ_{TOP}	0.8
Porosity, lower boundary, ϕ_{BOT}	0.2
Attenuation coefficient, *const*	1×10^{-5} cm^{-1}
Sediment burial velocity, lower boundary, ω_{BOT}	0.01 cm a^{-1}
Upward fluid velocity, v_{TOP}	0–0.3 cm a^{-1}
Rate constant for Li precipitation, k_{PPT}	1×10^{-4} a^{-1}
Li concentration, sediment surface, $[\mathrm{Li}]_{TOP}$	26 μM
Li concentration, lower boundary, $[\mathrm{Li}]_{BOT}$	2600 μM
δ^7Li, sediment surface	+31‰
δ^7Li, lower boundary	+0.3‰

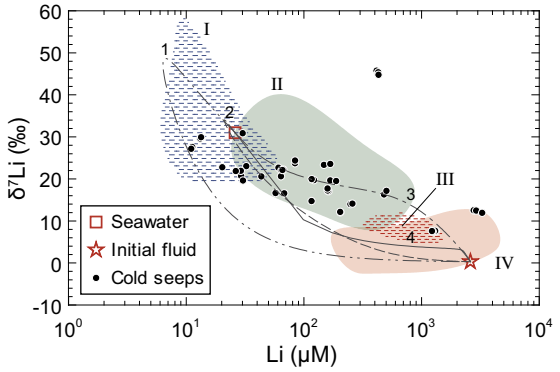

Fig. 6. Plot of δ^7Li versus Li concentration showing results of the transport-reaction modeling. Note logarithmic scale of x-axis. The model simulates Li isotope fractionation during vertical transport of deep-seated pore fluids to the seafloor at different upward advection rates: 1, $v_{TOP} = 0.0$ cm a^{-1}; 2, $v_{TOP} = 0.003$ cm a^{-1}; 3, $v_{TOP} = 0.03$ cm a^{-1}; 4, $v_{TOP} = 0.3$ cm a^{-1}. Circles represent measured data of cold seep fluids. The colored domains depict the compositional ranges of reference fluid types: I, low-temperature diagenesis; II, high-temperature diagenesis; III, ridge-crest hydrothermal systems; IV, sediment-hosted hydrothermal systems.

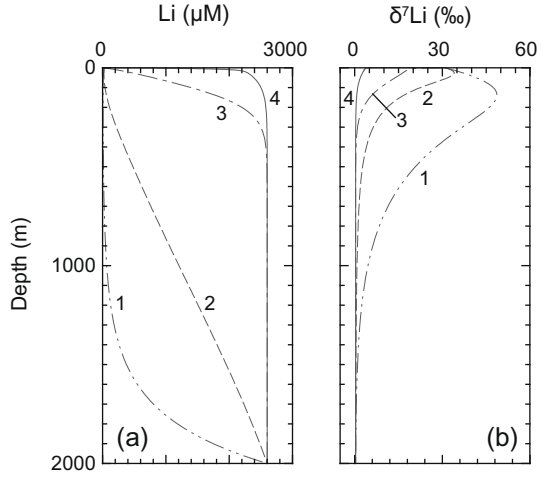

Fig. 7. Pore water profiles of Li concentration (a) and δ^7Li (b) showing results of the transport-reaction modeling: 1, $v_{TOP} = 0.0$ cm a^{-1}; 2, $v_{TOP} = 0.003$ cm a^{-1}; 3, $v_{TOP} = 0.03$ cm a^{-1}; 4, $v_{TOP} = 0.3$ cm a^{-1}. Although the modeled scenarios do not correspond to pore water profiles at specific sites, the figure illustrates how the composition of fluids close to the upper boundary (i.e., in the cold seeps) changes with changing advection rates.

traverses the lower half of the high-temperature diagenetic domain and follows the major trend of cold seep fluids (curve 3; Fig. 6). The mixing zone between seawater and the original deep fluid is shifted into the uppermost 200 m of the modeled sediment column (Fig. 7). This demonstrates that moderate pore water movement suffices to transmit a considerable portion of the deep-seated Li isotope signal into shallow sediments.

Increasing the advection rate by another order of magnitude results in Li concentrations and δ^7Li values equal to that of the original deep fluid in the entire sediment column (curve 4; Figs. 6 and 7). This is in agreement with field observations at the eastern flank of the Juan de Fuca Ridge where hydrothermal basement fluids percolate through up to 900 m thick hemipelagic sediments. Because of low basement temperatures, the original Li concentration of fluids in that area is quite different from the one adopted in the present model. Nonetheless, Wheat and Mottl (2000) demonstrated, based on a comparative study of spring and pore fluids, that almost unaltered basement fluids may reach the top of the sediment column if fluid advection rates exceed a few mm a^{-1}. In an analogous manner, preservation of the deep-seated Li signal in fluids of Dvurechenskii MV may be explained with the high fluid advection rates prevailing at this site (Figs. 2t and 3b; Aloisi et al., 2004). Higher temperatures at the model boundaries would further decrease Li precipitation during upward transport and, thus, result in an even more pristine isotope signal at the sediment surface. The effect of high temperatures (>300 °C) and advection rates on the δ^7Li of pore fluids is clearly demonstrated at Swallow Chimney, Okinawa Trough (Fig. 3). At this site, rapid upward transport of fluids has pushed the mixing zone between seawater and hydrothermal pore fluids beyond the sediment/bottom water interface (Fig. 2d) and the δ^7Li values are the lightest observed throughout this study.

6. SUMMARY AND CONCLUSIONS

In the present study, we evaluated the applicability of Li isotope systematics as a tracer for the origin and diagenetic evolution of pore fluids at cold seeps and similar submarine fluid escape structures. For that purpose, we established a general reference frame for Li isotope fractionation in marine systems. The major findings are summarized as follows:

(1) Literature data for fluids from bare ridge-crest and sediment-hosted hydrothermal systems as well as interstitial waters from normal ODP cores show a pronounced negative correlation between δ^7Li and Li concentration reflecting Li release from sediments or rocks and/or uptake of Li during clay mineral authigenesis.

(2) Most cold seep fluids are in good agreement with this general trend and show higher Li concentrations and lower δ^7Li values than seawater. A common signal of clay mineral dehydration in most cold seep fluids indicates that diagenetic smectite/illite is the major sink for light pore water Li. Deviations from the general correlation trend are attributed to particularities in sediment composition and to transport-related fractionation mechanisms.

(3) Pore fluids on passive margins receive high amounts of Li from intensely weathered, terrigenous and continental material. In contrast, on convergent margins and in other settings with strong volcanogenic input, Li concentrations in pore water are lower because of intense Li uptake during alteration of volcanic glass and other labile components. In addition, adsorption of Li by smectite at low temperature may exert an important control on pore water Li in volcanogenic settings. Separate investigation in shallow sediments revealed that this process is not accompanied by isotope fractionation.

(4) The isotopic composition of two evolutionarily distinct Mediterranean brines is in good agreement with the general correlation trend. It is inferred that saline pore fluids are generally not affected by fractionation mechanisms specifically related to evaporation or evaporite dissolution.

(5) Application of a numerical transport-reaction model, simulating Li isotope fractionation during active upward transport of fluids, revealed that little upward advection suffices to transfer deep-seated diagenetic Li signals into shallow sediments. Once the advection rate exceeds a few mm a^{-1} (assuming normal sedimentation rates) deep fluids that are almost unaltered by shallow fractionation processes may reach the upper end of the sediment column. The modeling results show that, if carefully applied, Li isotope systematics of cold seep fluids may provide a valuable record of fluid/sediment or fluid/rock interaction that has been inherited several hundreds or thousands of meters below the seafloor.

ACKNOWLEDGMENTS

We would like to acknowledge the support of officers and crews during sea-going expeditions with RVs Aegeo, Marion Dufresne, Meteor, Pelagia, Poseidon and Sonne. Furthermore, we are grateful to our colleagues A. Bleyer, B. Domeyer, A. Kolevica, C. Schulz and R. Surberg for assistance with analytical work at sea and in land-based laboratories. Thorough reviews by P.B. Tomascak and two anonymous referees are greatly appreciated. This is Publication No. 185 of the Sonderforschungsbereich 574 "Volatiles and Fluids in Subduction Zones" at Kiel University. Financial support was obtained by RWE-Dea through R&D project West Nile Delta (WND) and by the Federal Ministry of Education and Research (BMBF) (Grant No. 03G0196B).

APPENDIX A. SUPPLEMENTARY DATA

Supplementary data associated with this article can be found, in the online version, at doi:10.1016/j.gca.2010.03.026.

REFERENCES

Aloisi G., Drews M., Wallmann K. and Bohrmann G. (2004) Fluid expulsion from the Dvurechenskii mud volcano (Black Sea). Part I. Fluid sources and relevance to Li, B, Sr, I and dissolved inorganic nitrogen cycles. *Earth Planet. Sci. Lett.* **225**, 347–363.

Berger G., Schott J. and Guy C. (1988) Behavior of Li, Rb and Cs during basalt glass and olivine dissolution and chlorite, smectite and zeolite precipitation from seawater: experimental investigations and modelization between 50 and 300 °C. *Chem. Geol.* **71**, 297–312.

Bernasconi S. M. (1999) Interstitial water chemistry in the western Mediterranean: results from leg 161. In *Proc. Oc. Drill. Prog. Sci. Res.*, vol. 131 (eds. R. Zahn, M. C. Comas and A. Klaus). Ocean Drilling Program, College Station, TX, pp. 423–432.

Berner R. A. (1980) *Early Diagenesis – A Theoretical Approach*. Princeton University Press, Princeton, NJ.

Bohrmann G., Ivanov M., Foucher J. P., Spiess V., Bialas J., Greinert J., Weinrebe W., Abegg F., Aloisi G., Artemov Y., Blinova V., Drews M., Heidersdorf F., Krabbenhöft A., Klaucke I., Krastel S., Leder T., Polikarpov I., Saburova M., Schmale O., Seifert R., Volkonskaya A. and Zillmer M. (2003) Mud volcanoes and gas hydrates in the Black Sea: new data from Dvurechenskii and Odessa mud volcanoes. *Geo-Mar. Lett.* **23**, 239–249.

Bottomley D. J., Katz A., Chan L. H., Starinsky A., Douglas M., Clark I. D. and Raven K. G. (1999) The origin and evolution of Canadian Shield brines: evaporation or freezing of seawater? New lithium isotope and geochemical evidence from the Slave craton. *Chem. Geol.* **155**, 295–320.

Boudreau B. P. (1996) The diffusive tortuosity of fine-grained unlithified sediments. *Geochim. Cosmochim. Acta* **60**, 3139–3142.

Boudreau B. P. (1997) *Diagenetic Models and their Implementation*. Springer-Verlag, Berlin.

Butterfield, D.A., McDuff, R.E., Franklin, J. and Wheat, C.G. (1994) Geochemistry of hydrothermal vent fluids from Middle Valley Juan de Fuca Ridge. In *Proc. Oc. Drill. Prog. Sci. Res.*, vol. 139 (eds. J. Mottl, E.E. Davis, A.T. Fisher and J.F. Slack). Ocean Drilling Program, College Station, TX, pp. 395–410.

Castrec M., Dia A. N. and Boulègue J. (1996) Major- and trace-element and Sr isotope constraints on fluid circulation in the Barbados accretionary complex. Part II. Circulation rates and fluxes. *Earth Planet. Sci. Lett.* **142**, 487–499.

Camerlenghi A., Cita M. B., Hieke W. and Ricchiuto T. (1992) Geological evidence for mud diapirism on the Mediterranean Ridge accretionary complex. *Earth Planet. Sci. Lett.* **109**, 493–504.

Chan L. H. and Kastner M. (2000) Lithium isotopic compositions of pore fluids and sediments in the Costa Rica subduction zone: implications for fluid processes and sediment contribution to the arc volcanoes. *Earth Planet. Sci. Lett.* **183**, 275–290.

Chan L. H., Edmond J. M. and Thompson G. (1993) A lithium isotope study of hot springs and metabasalts from mid-ocean ridge hydrothermal systems. *J. Geophys. Res.* **98**, 9653–9659.

Chan L. H., Gieskes J. M., You C. F. and Edmond J. M. (1994) Lithium isotope geochemistry of sediments and hydrothermal fluids of the Guaymas Basin, Gulf of California. *Geochim. Cosmochim. Acta* **58**, 4443–4454.

Chan L. H., Starinsky A. and Katz A. (2002) The behavior of lithium and its isotopes in oilfield brines: evidence from the Heletz-Kokhav field, Israel. *Geochim. Cosmochim. Acta* **66**, 615–623.

Chan L. H., Leeman W. P. and Plank T. (2006) Lithium isotopic composition of marine sediments. *Geochem. Geophys. Geosyst.* **7**, QO6005. doi:10.1029/2005GC001202.

Dählmann A. and De Lange G. J. (2003) Fluid-sediment interactions at Eastern Mediterranean mud volcanoes: a stable isotope study from ODP Leg 160. *Earth Planet. Sci. Lett.* **212**, 377–391.

Davie M. K. and Buffett B. A. (2003) Sources of methane gas hydrate: inferences from a comparison of observations and numerical models. *Earth Planet. Sci. Lett.* **206**, 51–56.

Davis E. E., Fisher A. T., Firth J. V. and Shipboard Scientific Party (1997) 1. Introduction and summary: hydrothermal circulation in the oceanic crust and its consequences on the eastern flank of the Juan de Fuca Ridge. In *Proc. Oc. Drill. Prog. Init. Rep.*, vol. 168 (eds. E. E. Davis, A. T. Fisher and J. V. Firth). Ocean Drilling Program, College Station, TX, pp. 7–21.

De Lange G. J., Middelburg J. J., Van der Weijden C. H., Catalano G., Luther, III, G. W., Hydes D. J., Woittiez J. R. W. and Klinkhammer G. P. (1990) Composition of anoxic hypersaline brines in the Tyro and Bannock Basins, eastern Mediterranean. *Mar. Chem.* **31**, 63–88.

Fehn U., Snyder G. T. and Muramatsu Y. (2007) Iodine as a tracer of organic material: ^{129}I results from gas hydrate systems and fore arc fluids. *J. Geochem. Explor.* **95**, 66–80.

Fisher A. T. (2004) Rates of flow and patterns of fluid circulation. In *Hydrogeology of the Oceanic Lithosphere* (eds. E. E. Davis and H. Elderfield). Cambridge University Press, Cambridge, pp. 337–375.

Flesch G. D., Anderson, Jr., A. R. and Svec H. J. (1973) A secondary isotopic standard for ^{6}Li/^{7}Li determinations. *Int. J. Mass Spectrom. Ion Proc.* **12**, 265–272.

Fontes J. C. and Matray J. M. (1993) Geochemistry and origin of formation brines from the Paris Basin, France. 1. Brines associated with Triassic salts. *Chem. Geol.* **109**, 149–175.

Foucault A. and Stanley D. J. (1989) Late Quaternary palaeoclimatic oscillations in East Africa recorded by heavy minerals in the Nile delta. *Nature* **339**, 44–46.

Fouquet Y., Zierenberger R. A., Miller D. J. and Shipboard Scientific Party (1998) 1. Introduction: investigation of hydrothermal circulation and genesis of massive sulfide deposits at sediment-covered spreading centers at Middle Valley and Escanaba Trough. In *Proc. Oc. Drill. Prog. Init. Rep.*, vol. 169 (eds. Y. Fouquet, R. A. Zierenberger and D. J. Miller). Ocean Drilling Program, College Station, TX, pp. 7–15.

Foustoukos D. I., James R. H., Berndt M. E. and Seyfried J. W. E. (2004) Lithium isotopic systematics of hydrothermal vent fluids

at the Main Endeavour Field, Northern Juan de Fuca Ridge. *Chem. Geol.* **212**, 17–26.

Gieskes J. M. and Mahn C. (2007) Halide systematics in interstitial waters of ocean drilling sediment cores. *Appl. Geochem.* **22**, 515–533.

Glasby G. P. and Notsu K. (2003) Submarine hydrothermal mineralization in the Okinawa Trough, SW of Japan: an overview. *Ore Geol. Rev.* **23**, 299–339.

Grasshoff K., Erhardt M. and Kremling K. (2002) *Methods of Seawater Analysis*. Wiley-VCH, Weinheim.

Griffin J. J., Windom H. and Goldberg E. D. (1968) The distribution of clay minerals in the world ocean. *Deep-Sea Res. I* **15**, 433–459.

Haese R. R., Hensen C. and De Lange G. J. (2006) Pore water geochemistry of eastern Mediterranean mud volcanoes: implications for fluid transport and fluid origin. *Mar. Geol.* **22**, 191–208.

Hensen C. and Wallmann K. (2005) Methane formation at Costa Rica continental margin – constraints for gas hydrate inventories and cross-décollement fluid flow. *Earth Planet. Sci. Lett.* **236**, 41–60.

Hensen C., Wallmann K., Schmidt M., Ranero C. R. and Suess E. (2004) Fluid expulsion related to mud extrusion off Costa Rica – a window to the subducting slab. *Geology* **32**, 201–204.

Hensen C., Nuzzo M., Hornibrook E., Pinheiro L. M., Bock B., Magalhães V. H. and Brückmann W. (2007) Sources of mud volcano fluids in the Gulf of Cadiz – indications for hydrothermal imprint. *Geochim. Cosmochim. Acta* **71**, 1232–1248.

Hyndman R. D. and Davis E. E. (1992) A mechanism for the formation of methane hydrate and seafloor bottom-simulating reflectors by vertical fluid expulsion. *J. Geophys. Res.* **97**, 7025–7041.

Huh Y., Chan L. H., Zhang L. and Edmond J. M. (1998) Lithium and its isotopes in major world rivers: implications for weathering and the oceanic budget. *Geochim. Cosmochim. Acta* **62**, 2039–2051.

Ishikawa T. and Nakamura E. (1993) Boron isotope systematics of marine sediments. *Earth Planet. Sci. Lett.* **117**, 567–580.

James R. H. and Palmer M. R. (2000) Marine geochemical cycles of the alkali elements and boron: the role of sediments. *Geochim. Cosmochim. Acta* **64**, 3111–3122.

James R. H., Rudnicki M. D. and Palmer M. R. (1999) The alkali element and boron geochemistry of the Escanaba Trough sediment-hosted hydrothermal system. *Earth Planet. Sci. Lett.* **171**, 157–169.

James R. H., Allen D. E. and Seyfried W. E. (2003) An experimental study of alteration of oceanic crust and terrigenous sediments at moderate temperatures (51–350 °C): insights as to chemical processes in near-shore ridge-flank hydrothermal systems. *Geochim. Cosmochim. Acta* **67**, 681–691.

Jeffcoate A. B., Elliot T., Thomas A. and Bouman C. (2004) Precise, small sample size determinations of lithium isotopic compositions of geological reference material and modern seawater by ICP-MS. *Geostand. Geoanal. Res.* **28**, 161–172.

Kastner M. and Rudnicki M. D. (2004) Ridge flank sediment–fluid interactions. In *Hydrogeology of the Oceanic Lithosphere* (eds. E. E. Davis and H. Elderfield). Cambridge University Press, Cambridge, pp. 534–571.

Kastner M., Elderfield H. and Martin J. B. (1991) Fluids in Convergent Margins: what do we know about their composition, origin, role in diagenesis and importance for oceanic chemical fluxes. *Philos. Trans. R. Soc. Lond. A* **335**, 243–259.

Kimura, G., Silver, E.A., Blum, P. and Shipboard Scientific Party (1997) 3. Site 1039. In *Proc. Oc. Drill. Prog. Init. Rep.*, vol. 170 (eds. G. Kimura, E.A. Silver and P. Blum). Ocean Drilling Program, College Station, TX, pp. 45–93.

Kısakürek B., James R. H. and Harris N. B. W. (2005) Li and δ^7Li in Himalayan rivers: proxies for silicate weathering. *Earth Planet. Sci. Lett.* **237**, 387–401.

Konno U., Tsunogai U., Nakagawa F., Nakaseama M., Ishibashi J. I., Nunoura T. and Nakamura K. I. (2006) Liquid CO_2 venting on the seafloor: Yonaguni Knoll IV hydrothermal system, Okinawa Trough. *Geophys. Res. Lett.* **33**, L16607. doi:10.1029/2006GL026115.

Kopf A. J. (2002) Significance of mud volcanism. *Rev. Geophys.* **40**, 1005. doi:10.1029/2000RG000093.

Limonov A. F., VanWeering T. C. E., Kenyon N. H., Ivanov M. K. and Meisner L. B. (1997) Seabed morphology and gas venting in the Black Sea mud volcano area: observations with the MAK-1 deep-tow side scan sonar and bottom profiler. *Mar. Geol.* **137**, 121–136.

Loncke L. and Mascle J.Fanil Scientific Parties (2004) Mud volcanoes, gas chimneys, pockmarks and mounds in the Nile deep-sea fan (Eastern Mediterranean): geophysical evidences. *Mar. Petrol. Geol.* **21**, 669–689.

Loncke L., Gaullier V., Mascle J., Vendeville B. and Camera L. (2006) The Nile deep-sea fan: an example of interacting sedimentation, salt tectonics, and inherited subsalt paleotopographic features. *Mar. Petrol. Geol.* **23**, 297–315.

Martin J. B., Kastner M. and Elderfield H. (1991) Lithium: sources in pore fluids of Peru slope sediments and implications for oceanic fluxes. *Mar. Geol.* **102**, 281–292.

Medialdea T., Somoza L., Pinheiro L. M., Fernández-Puga M. C., Vázquez J. T., León R., Ivanov M. K., Magalhaes V., Díaz-del-Río V. and Vegas R. (2009) Tectonics and mud volcano development in the Gulf of Cádiz. *Mar. Geol.* **261**, 48–63.

Millot R., Guerrot C. and Vigier N. (2004) Accurate and high-precision measurement of lithium in two reference materials by MC-ICP-MS. *Geostand. Geoanal. Res.* **28**, 153–159.

Moore J. C. and Vrolijk P. (1992) Fluids in accretionary prisms. *Rev. Geophys.* **30**, 113–135.

Müller D. W. and Mueller P. A. (1991) Origin and age of the Mediterranean Messinian evaporites: implications from Sr isotopes. *Earth Planet. Sci. Lett.* **107**, 1–12.

Nikishin A. M., Korotaev M. V., Ershov A. V. and Brunet M. F. (2003) The Black Sea basin: tectonic history and Neogene-Quaternary rapid subsidence modelling. *Sed. Geol.* **156**, 149–168.

Pinheiro L. M., Ivanov M., Kenyon N., Maghalães V., Somoza L., Gardner J., Kopf A., Van Rensbergen P. and Monteiro J.the Euromargins-MVSEIS Team (2005) Structural control of mud volcanism and hydrocarbon-rich fluid seepage in the Gulf of Cadiz: results from TTR-15 and previous cruises. *CIESM Workshop Monogr.* **29**, 53–58.

Pistiner J. S. and Henderson G. M. (2003) Lithium-isotope fractionation during continental weathering processes. *Earth Planet. Sci. Lett.* **214**, 327–339.

Pogge von Strandmann P. A. E., James R. H., van Calsteren P., Gíslason S. R. and Burton K. (2008) Lithium, magnesium and uranium isotope behaviour in the estuarine environment of basaltic islands. *Earth Planet. Sci. Lett.* **274**, 462–471.

Pogge von Strandmann P. A. E., Burton K., James R. H., van Calsteren P. and Gíslason S. R. (2010) Assessing the role of climate on uranium and lithium behaviour in rivers draining a basaltic terrain. *Chem. Geol.* **270**, 227–239.

Ranero C. R. and Von Huene R. (2000) Subduction erosion along the Middle America convergent margin. *Nature* **404**, 748–752.

Reitz A., Haeckel M., Wallmann K., Hensen C. and Heeschen K. (2007) Origin of salt-enriched pore fluids in the northern Gulf of Mexico. *Earth Planet. Sci. Lett.* **259**, 266–282.

Roberts H. H. and Carney R. S. (1997) Evidence of episodic fluid, gas, and sediment venting on the northern Gulf of Mexico

continental slope. *Econ. Geol. Bull. Soc. Econ. Geol.* **92**, 863–879.

Robertson A. H. F.Ocean Drilling Program Leg 160 Scientific Party (1996) Mud volcanism on the Mediterranean Ridge: initial results of Ocean Drilling Program Leg 160. *Geology* **24**, 239–242.

Robertson A. H. F. and Kopf A. (1998) 50. Tectonic setting and processes of mud volcanism on the Mediterranean Ridge accretionary complex: evidence from leg 160. In *Proc. Oc. Drill. Prog. Sci. Res.*, vol. 160 (eds. A. H. F. Robertson, K.-C. Emeis, C. Richter and A. Camerlenghi). Ocean Drilling Program, College Station, TX, pp. 665–680.

Ryan W. B. F., Venkatarathnam K. and Wezel F. C. (1973) 25.2. Mineralogical composition of the Nile Cone, Mediterranean Ridge, and Strabo Trench sandstones and clays. In *Init. Rep. Deep Sea Drill. Proj.*, vol. 13. US Government Printing Office, Washington, DC, pp. 731–745.

Rudnick R. L., Tomascak P. B., Njo H. B. and Gardner L. R. (2004) Extreme lithium isotopic fractionation during continental weathering revealed in saprolites from South California. *Chem. Geol.* **212**, 45–57.

Scholz F., Hensen C., Reitz A., Romer R. L., Liebetrau V., Meixner A., Weise S. M. and Haeckel M. (2009) Isotopic evidence ($^{87}Sr/^{86}Sr$, δ^7Li) for alteration of the oceanic crust at deep-rooted mud volcanoes in the Gulf of Cadiz, NE Atlantic Ocean. *Geochim. Cosmochim. Acta* **73**, 5444–5459.

Sonnenfeld P. (1984) *Brines and Evaporites*. Academic Press, New York.

Spinelli G. A. and Underwood M. B. (2004) Character of sediments entering the Costa Rica subduction zone: implications for partitioning of water along the plate interface. *The Island Arc* **13**, 432–451.

Środoń J. (1999) Nature of mixed-layer clays and mechanisms of their formation and alteration. *Annu. Rev. Earth Planet. Sci.* **27**, 19–53.

Stoffers P. and Müller G. (1978) 7. Mineralogy and lithofacies of Black Sea sediments Leg 42B Deep-sea Drilling Project. In *Init. Rep. Deep Sea Drill. Proj.*, vol. 42. US Government Printing Office, Washington, DC, pp. 373–411.

Stumm W. and Morgan J. J. (1995) *Aquatic chemistry: chemical equilibria and rates in natural waters*. Wiley-VCH, Weinheim.

Teng F. Z., McDonough W. F., Rudnick R. L., Dalpe C., Tomascak P. B., Chappell B. W. and Gao S. (2004) Lithium isotopic composition and concentration of the upper continental crust. *Geochim. Cosmochim. Acta* **68**, 4167–4178.

Tomascak P. B., Carlson R. W. and Shirley S. B. (1999) Accurate and precise determination of Li isotopic compositions by multi-collector sector ICP-MS. *Chem. Geol.* **158**, 145–154.

Tomascak P. B., Langmuir C. H., Le Roux P. J. and Shirley S. B. (2008) Lithium isotopes in global mid-ocean ridge basalts. *Geochim. Cosmochim. Acta* **72**, 1626–1637.

Vengosh A., De Lange G. J. and Starinsky A. (1998) Boron isotope and geochemical evidence for the origin of Urania and Bannock brines at the eastern Mediterranean: effect of water–rock interactions. *Geochim. Cosmochim. Acta* **62**, 3221–3228.

Venkatarathnam K. and Ryan W. B. F. (1971) Dispersal patterns of clay minerals in the sediments of the eastern Mediterranean Sea. *Mar. Geol.* **11**, 261–282.

Vigier N., Decarreau A., Millot R., Carignan J., Petit S. and France-Lanord C. (2008) Quantifying Li isotope fractionation during smectite formation and implications for the Li cycle. *Geochim. Cosmochim. Acta* **72**, 780–792.

Wallmann K., Suess E., Westbrook G. H., Winckler G. and Cita M. B. (1997) Salty brines on the Mediterranean sea floor. *Nature* **387**, 31–32.

Wallmann K., Drews M., Aloisi G. and Bohrmann G. (2006a) Methane discharge into the Black Sea and the global ocean via fluid flow through submarine mud volcanoes. *Earth Planet. Sci. Lett.* **248**, 545–560.

Wallmann K., Aloisi G., Haeckel M., Obzhirov A., Pavlova G. and Tishchenko P. (2006b) Kinetics of organic matter degradation, microbial methane generation, and gas hydrate formation in anoxic marine sediments. *Geochim. Cosmochim. Acta* **70**, 3905–3972.

Wallmann K., Aloisi G., Haeckel M., Tishchenko P., Pavlova G., Greinert J., Kutterolf S. and Eisenhauer A. (2008) Silicate weathering in anoxic marine sediments. *Geochim. Cosmochim. Acta* **72**, 2895–2918.

Wedepohl K. H. (1978) *Handbook of Geochemistry II*. Springer-Verlag, Berlin.

Wheat C. G. and Mottl M. J. (2000) Composition of pore and spring waters from Baby Bare: global implications of geochemical fluxes from a ridge flank hydrothermal system. *Geochim. Cosmochim. Acta* **64**, 629–642.

Williams L. B. and Hervig R. L. (2005) Lithium and boron isotopes in illite–smectite: the importance of crystal size. *Geochim. Cosmochim. Acta* **69**, 5705–5716.

Wunder B., Meixner A., Romer R. L. and Heinrich W. (2006) Temperature-dependent isotopic fractionation of lithium between clinopyroxene and high-pressure hydrous fluids. *Contrib. Mineral. Petrol.* **151**, 112–120.

Wunder B., Meixner A., Romer R. L., Feenstra A., Schettler G. and Heinrich W. (2007) Lithium isotope fractionation between Li-bearing staurolite, Li-mica and aqueous fluids: an experimental study. *Chem. Geol.* **238**, 277–290.

You C. F., Chan L. H., Spivack A. J. and Gieskes J. M. (1995) Lithium, boron, and their isotopes in sediments and pore waters of Ocean Drilling Program Site 808, Nankai Trough: implications for fluid expulsion in accretionary prisms. *Geology* **23**, 37–40.

You C. F., Castillo P. R., Gieskes J. M., Chan L. H. and Spivack A. J. (1996) Trace element behavior in hydrothermal experiments: implications for fluid processes at shallow depths in subduction zones. *Earth Planet. Sci. Lett.* **140**, 41–52.

You C. F., Chan L. H., Gieskes J. M. and Klinkhammer G. P. (2003) Seawater intrusion through the oceanic crust and carbonate sediment in the Equatorial Pacific: lithium abundance and isotopic evidence. *Geophys. Res. Lett.* **30**. doi:10.1029/2003GL018412.

Zhang L., Chan L. H. and Gieskes J. M. (1998) Lithium isotope geochemistry of pore waters from ocean drilling program Sites 918 and 919, Irminger Basin. *Geochim. Cosmochim. Acta* **62**, 2437–2450.

Zitter T. A. C., Huguen C. and Woodside J. M. (2005) Geology of mud volcanoes in the eastern Mediterranean from combined sidescan sonar and submersible surveys. *Deep-Sea Res. I* **52**, 457–475.

Associate editor: Jeffrey C. Alt